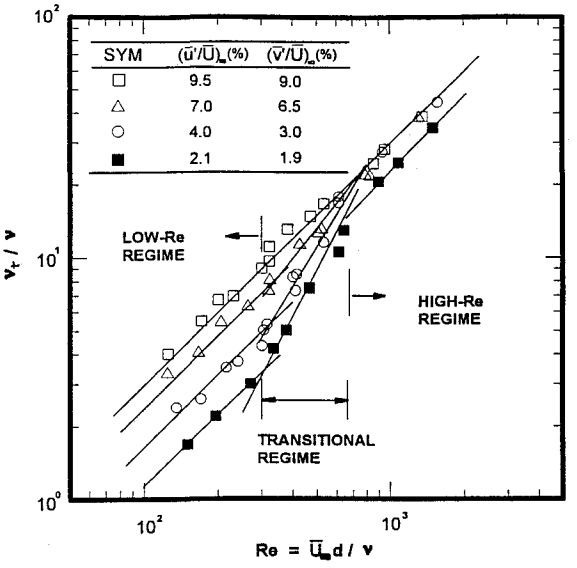

Fig. 3 Variation of turbulence viscosity with sphere Reynolds number and ambient turbulence intensity.

linear for a particular value of $(\bar{u}'/\bar{U})_\infty$ in the low Re range, with values progressively increasing as $(\bar{u}'/\bar{U})_\infty$ increases. This behavior can be explained based on crude mixing-length concepts of turbulent transport, e.g., $\nu_t - \nu \sim \bar{v}'\ell$. Now $\bar{v}' \sim \bar{v}'_\infty$ before vortex shedding begins whereas $\ell \sim d$ since the sphere size tends to control the width of the flow in the critical region near the start of the laminar-like turbulent wake. Thus, $\nu_t - \nu \sim \bar{v}'d \approx (\bar{v}'/\bar{U})_\infty \bar{U}_\infty d$ or $\nu_t/\nu - 1 \sim Re(\bar{v}'/\bar{U})_\infty$. This implies that ν_t/ν should increase linearly with both increasing Re and $(\bar{v}'/\bar{U})_\infty \sim (\bar{u}'/\bar{U})_\infty$, similar to the behavior observed in Fig. 3.

The variation of ν_t/ν also is nearly linear in Re in the high Re regime but is less dependent on the ambient turbulence intensity. This behavior can be explained by invoking the same mixing-length argument as before although noting that $\nu_t \gg \nu$ in the high Re regime. Then, $\nu_t/\nu \sim \bar{v}'\ell/\nu$ and in the laminar-like turbulent wake, $\bar{v}' \sim \bar{U}_\infty \gg \bar{v}'_\infty$. Estimating $\ell \sim d$, as before, then yields $\nu_t/\nu \sim \bar{U}_\infty d/\nu = Re$, generally, as observed in Fig. 3. As a result, ν_t/ν mainly is independent of $(\bar{v}'/\bar{U})_\infty \sim (\bar{u}'/\bar{U})_\infty$ in this high Re regime although the presence of ambient turbulence is needed to initiate laminar-like turbulent wake behavior. Finally, for an ambient turbulence intensity of 9.5%, effects of vortex shedding are suppressed due to the high-turbulence levels, as discussed earlier, so that high Re behavior persists to the smallest Re considered. Whether this behavior is representative of all higher ambient turbulence levels, as suggested by behavior in the high Re regime, is an interesting issue that should be resolved.

The rate of increase of ν_t/ν with increasing Re is more rapid in the transition regime than in the other two regimes [except when $(\bar{u}'/\bar{U})_\infty = 9.5\%$ which was just discussed]. Properties of ν_t/ν are most complex in this regime since its limits at low and high Re must accommodate rather different responses to variations of ambient turbulence intensities.

Conclusions

The present study considered sphere wakes for $Re = 125$–1560, $(\bar{u}'/\bar{U})_\infty = 2.0$–$9.5\%$, and ratios of the ambient integral and Kolmogorov length scales to d in the ranges 8–59 and 0.05–1.08, respectively. The major conclusions are as follows. 1) The wakes were turbulent but scaled like self-preserving laminar wakes with enhanced viscosities due to the presence of turbulence. 2) The effective turbulent viscosities were relatively independent of position and ratios of ambient integral and Kolmogorov length scales to d, however, they varied with both Re and $(\bar{u}'/\bar{U})_\infty$ in a low Reynolds number regime ($Re < 300$) and with Re alone in a high Reynolds number regime ($Re > 600$), with the transition regime between them associated with significant effects of vortex shedding from the sphere. 3) The laminar-like turbulent wake region was followed by a final decay region beginning when $\bar{u}_c \sim \bar{u}'_\infty$, which exhibits faster decay rates than any other axisymmetric wake observed thus far.

Acknowledgments

This research was sponsored by the Air Force Office of Scientific Research, Air Force Systems Command, USAF, under Grant F49620-92-J-0399.

References

[1]Mizukami, M., Parthasarathy, R. N., and Faeth, G. M., "Particle-Generated Turbulence in Homogeneous Dilute Dispersed Flows," *International Journal of Multiphase Flow*, Vol. 18, No. 3, 1992, pp. 397–412.

[2]Wu, J.-S., and Faeth, G. M., "Sphere Wakes in Still Surroundings at Intermediate Reynolds Numbers," *AIAA Journal*, Vol. 31, No. 8, 1993, pp. 1448–1455.

[3]Wu, J.-S., and Faeth, G. M., "Sphere Wakes at Moderate Reynolds Numbers in a Turbulent Environment," *AIAA Journal*, Vol. 32, No. 3, 1993, pp. 535–541.

[4]Wu, J.-S., "The Structure of Sphere Wakes at Intermediate Reynolds Numbers in Still and Turbulent Environments," Ph.D. Thesis, Department of Aerospace Engineering, Univ. of Michigan, Ann Arbor, MI, 1994.

[5]Tennekes, H., and Lumley, J. L., *A First Course in Turbulence*, Massachusetts Inst. of Technology Press, Cambridge, MA, 1972, pp. 113–124.

[6]Schlichting, H., *Boundary Layer Theory*, 7th ed., McGraw-Hill, New York, 1977, pp. 234–235 and 599.

Hypersonic Shock-Induced Combustion in a Hydrogen-Air System

J. K. Ahuja* and S. N. Tiwari†
Old Dominion University, Norfolk, Virginia 23529
and
D. J. Singh‡
Analytical Services and Materials, Inc., Hampton, Virginia 23666

Introduction

FOR an efficient propulsion system at hypersonic speeds, the combustion must take place at supersonic speeds. One of the proposed modes of propulsion is the shock-induced combustion ramjet (shramjet) in which a shock is employed to increase the temperature of premixed fuel and air to a point where chemical reaction will start. Apparent advantages of the shramjet over the scramjet engine include very short-length combustors and simple engine geometries. The phenomena of shock induced combustion/detonation around bodies traveling at hypersonic speeds is of great theoretical interest because of the need to understand the basic mechanism of combustion instabilities.

In the past, many researchers have conducted ballistic range experiments to study supersonic combustion/detonation. In these experiments, projectiles were fired in different premixed fuel air mixtures, and detonation structures around the projectiles were recorded. Every gas mixture has a detonation wave velocity known as Chapman-Jouget (C-J) velocity, which is characteristic of the mixture. If the velocity of the projectile is above the C-J velocity of the reactive mixture, the freestream velocity is referred to as overdriven. On the other hand, if the projectile velocity is lower than the C-J velocity, the freestream velocity is referred to as underdriven. For a given projectile diameter, the detonation wave structure is

Received Nov. 27, 1993; revision received April 12, 1994; accepted for publication Aug. 10, 1994.

*Graduate Research Assistant, Department of Mechanical Engineering. Student Member AIAA.

†Eminent Professor, Department of Mechanical Engineering. Associate Fellow AIAA.

‡Senior Research Scientist. Member AIAA.

highly unstable for projectile velocities less than the C-J velocity of the mixture. If the projectile is flying above the C-J velocity of the gas mixture, the detonation or reaction front structure shows a coupled shock-deflagration system near the stagnation line of the body. These two fronts separate from each other as one moves away from the stagnation line. The separation between the two fronts occurs as soon as the velocity component normal to the bow shock is equal to the detonation velocity. The separation between the bow shock and the reaction front is called the induction zone.

In 1972 Lehr[1] conducted a detailed experimental study for a wide range of projectile shapes and combustible mixtures. The mixture included hydrogen-air, hydrogen-oxygen, methane-air, and methane-oxygen. Lehr's experimental ballistic range shadowgraphs for Mach 5.11 and Mach 6.46 are given in Refs. 1 and 2. In both cases, a freestream temperature of 292 K and a pressure of 42663.2 N/m^2 (320 mm of Hg) is used along with a stoichiometric mixture of hydrogen-air. The shadowgraph for the Mach 5.11 case, which is at the C-J speed of the mixture, shows corrugations in the reaction front. These corrugations are caused by the pulsation of the reaction front. The frequency of this pulsation was determined to be 1.96 MHz, whereas for the Mach 6.46 case, it is seen that the reaction front is coupled with the shock near the stagnation line and up to about 60–65-deg body angle from the stagnation line. This is because of a very high postshock temperature at Mach 6.46 which causes the induction zone to become very narrow. Consequently, it appears that the two fronts are merged with each other. Decoupling begins farther downstream from the stagnation line when the postshock temperature starts decreasing and, therefore, the induction distance increases. Further, both the bow shock and the reaction fronts are smooth without any visible instabilities. Thus, for an overdriven case of Mach 6.46, the instabilities have disappeared. Results for other underdriven cases are available in Refs. 1 and 2, and they demonstrate that the instabilities in the reaction front become more pronounced as the projectile velocity is reduced below the C-J velocity of the mixture. In all these cases the projectile diameter was fixed as 15 mm.

Several researchers have attempted to numerically simulate Lehr's ballistic range experiments. These are discussed in details in Refs. 3–13. The objective of this study is to investigate, in detail, the shock-induced combustion phenomena for the premixed stoichiometric H_2-air mixture flow at hypersonic speeds (Mach 5.11 and 6.46).

Theoretical Formulation and Solution Procedure

The physical problem considered here is a 15-mm spherical projectile flying at Mach 5.11 and 6.46 in a stoichiometric hydrogen-air mixture. In both the cases a freestream temperature of 292 K and a pressure of 320 mm of Hg is used. The flow conditions considered correspond to the cases experimentally investigated by Lehr.[1]

The physical model for analyzing the flowfield is described by the Navier-Stokes and species continuity equations. A seven-species, seven-reactions hydrogen-air combustion model due to Jachimowski[14] is used. The stoichiometric chemical reaction for a hydrogen-air system can be written as

$$2H_2 + O_2 + 3.76N_2 \rightarrow 2H_2O + 3.76N_2$$

The species are N_2, O_2, H_2, OH, H_2O, O, and H. Each of the seven reactions can proceed in the forward and backward directions. The reactions are

$$O_2 + H_2 \rightleftharpoons OH + OH \quad (1)$$

$$O_2 + H \rightleftharpoons OH + O \quad (2)$$

$$H_2 + OH \rightleftharpoons H_2O + H \quad (3)$$

$$H_2 + O \rightleftharpoons OH + H \quad (4)$$

$$OH + OH \rightleftharpoons H_2O + O \quad (5)$$

$$OH + H + M \rightleftharpoons H_2O + M \quad (6)$$

$$H + H + M \rightleftharpoons H_2 + M \quad (7)$$

The analysis is carried out using the axisymmetric version of the SPARK2D code,[15] which incorporates the preceding combustion model. The governing equations are solved using MacCormack's[16] method. The scheme is second-order accurate in time and space. This results in a spatially and temporally discrete, simultaneous system of equations at each grid point. The system of equations is solved subject to initial and boundary conditions. At the supersonic inflow boundary, all flow quantities are specified as freestream conditions. At the supersonic outflow boundary, all flow quantities are extrapolated from interior grid points. Although full Navier-Stakes (N-S) equations are used, the slip conditions are used to numerically simulate the inviscid flow. A flow tangency or slip boundary condition is implied on the solid wall. The wall temperature and pressure are extrapolated from interior grid points. Initial conditions are obtained by specifying freestream conditions throughout the flowfield. The resulting set of equations is marched in time. The details of the governing equations and the method of solution are given in Ref. 15.

When a blunt body is moving through a reactive mixture at hypersonic speeds, a bow shock is formed ahead of the body, and the temperature of the fuel-air mixture after the bow shock is sufficiently high to initiate the reaction. Once the ignition starts, chemical energy is released and another discontinuity known as the reaction front is formed. The instability in the structure of the reaction front originates in the induction zone which separates the bow shock and the exothermic reaction front in the nose region of the flowfield and then spreads outward. In the induction zone, the temperature and the pressure remain relatively constant at the postshock conditions, whereas the concentrations of radicals build up very rapidly. To capture the physical instabilities, the calculations must be carried out for long times to ensure that all relevant time scales are being captured. Since all schemes have some numerical diffusion, which is dependent on the grid resolution, a coarse grid may damp out these oscillations. Further, the numerical damping added to the scheme in the vicinity of the reaction front may damp or alter the instability modes.

Because of the symmetry, only one-half of the flowfield is calculated. A typical grid used in the present calculations was 197 × 152 grid points (197 normal to the body and 152 along the body). For the present case of a stoichiometric hydrogen-air mixture, the Chapman-Jouget velocity is the same as the velocity of the projectile for the Mach 5.11 case. However, for the Mach 6.46 case, the projectile speed is significantly above the detonation velocity of the mixture. In the calculations for both cases, the residuals dropped by three orders in 12,000 iterations and then remained constant.

Results and Discussions

Results for Mach 5.11 is presented first. Figure 1 shows the contour plot of density. The bow shock and the reaction front can be

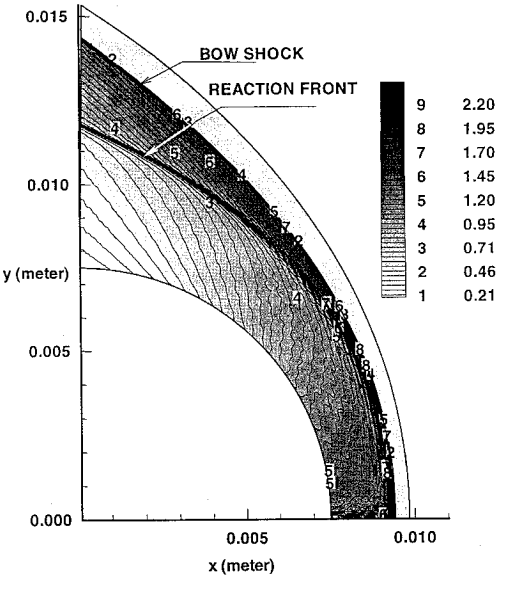

Fig. 1 Density contours for Mach 5.11.

seen clearly in the figure. They are separated from each other by the induction distance. The separation (i.e., the induction distance) is minimum near the stagnation line and increases away from it. This is because near the stagnation line, the bow shock is almost normal and, hence, the postshock temperature is maximum; thus, induction distance is minimum. Away from the stagnation line, the shock strength decreases, thereby decreasing the postshock temperature and, hence, increasing the induction distance. A comparison with the Lehr's shadowgraph[1,2] for Mach 5.11 shows that all of the flow features are very well captured. The bow shock is very crisp and smooth, whereas the reaction front is wrinkled. The pulsations or instabilities which arise at the stagnation point move all through the reaction front. The maximum density is seen to be just after the bow shock, and minimum density is after the reaction front. The shock standoff distance is comparable to the Lehr's shadowgraph.

The contour plots for the water mass fraction are shown in Fig. 2. At the end of the combustion zone, the temperature is high enough to start the combustion. As the reaction proceeds, the water mass fraction increases rapidly. The oscillations similar to temperature and density profiles can be seen. The instability is characterized by an almost regular periodic wave motion having a constant frequency. Similar instability has been observed experimentally in Lehr's work.

The instability in the reaction front has been explained in Ref. 3 by the wave interaction model as proposed by McVey and Toong[13] and as modified by Matsuo and Fujiwara.[9] The frequency of oscillations as determined by Fourier analysis and grid refinement studies was found to be 2.1 MHz (Ref. 5). The experimental frequency as found in Lehr's work was 1.96 MHz.

The results for the Mach 6.46 case will now be presented. As mentioned earlier, this is a superdetonative case, i.e., projectile velocity is higher than the detonation velocity of the mixture.

The temperature contours are shown in Fig. 3. Qualitatively the results are similar to the previous case except near the stagnation zone; the bow shock and the reaction front are now almost coupled due to very small induction distance (because of higher postshock temperature). The two fronts separate from each other slightly in the downstream region. Away from the stagnation line, the induction distance is increased as a result of decreasing shock strength and postshock temperature. The temperature further increases as the reaction proceeds due to the exothermic nature of the reaction. The peak temperature occurs at the stagnation point. The bow shock has a very crisp and smooth profile. The reaction front, which is smooth up to about 60–65 deg from the nose region, is wrinkled with very small amplitude waves downstream. A comparison with the Lehr's Mach 6.46 case shadowgraph[1] shows that all of the flow features are very well captured. The contour plot for the water mass fraction is shown in Fig. 4. The temperature is high enough to start the combustion at the end of the induction zone. The water mass fraction increases rapidly as the reaction proceeds. The figure also shows the

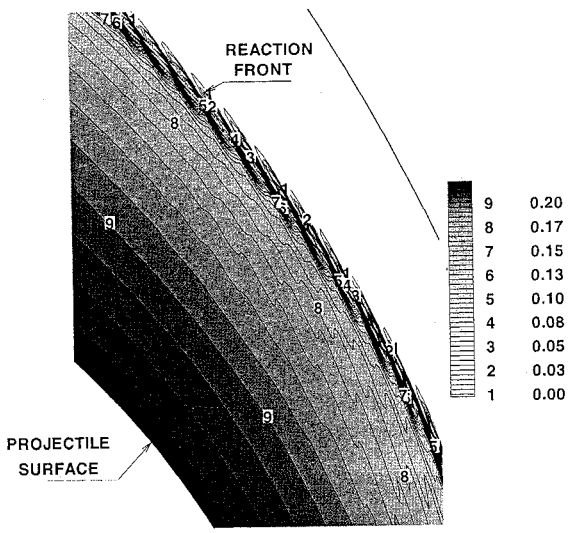

Fig. 2 Enlarged view of water mass fraction contours for Mach 5.11.

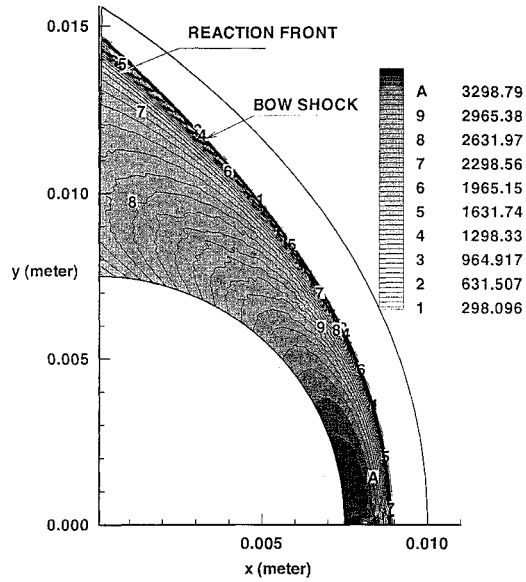

Fig. 3 Temperature contours for Mach 6.46.

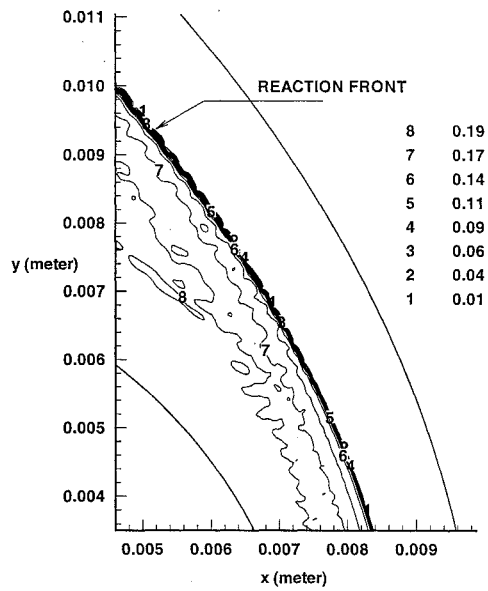

Fig. 4 Enlarged view of water mass fraction contours for Mach 6.46.

macroscopic behavior of the oscillations. The reaction front shows a smooth profile near the stagnation region, but a corrugated pattern with extremely small amplitudes is observed 60–70 deg away from the nose region.

A Fourier analysis of the flowfield was conducted to further investigate the macroscopic steady nature of the flowfield. For this, data at various sample stations for the 61 grid line along the body were stored for 30,000 iterations to get good temporal resolution. The grid used was 101 × 78, and all calculations were time accurate. Analysis of the flowfield spectrum showed a fundamental frequency of $1.28e + 6$ Hz and a peak amplitude of 0.001. It also showed subharmonics and high-frequency numerical noise. To get a grid independent solution the calculations were then repeated for a finer grid (131 × 101). The grid aspect ratio was kept the same, and the same physical locations were used as in the previous case. The dominant frequency calculated now was $2.63e + 6$ Hz, and the amplitude was 0.001. The calculations were repeated once again for yet another finer grid of 197 × 152. The grid aspect ratio was again kept the same, and the sample stations are at the same physical locations as in the previous cases. Figure 5 shows the frequency spectrum for this grid. The flowfield spectrum is well resolved, and it clearly shows the fundamental frequency of $2.67e + 6$ Hz and a peak amplitude of 0.001. Harmonics and very high-frequency numerical noise

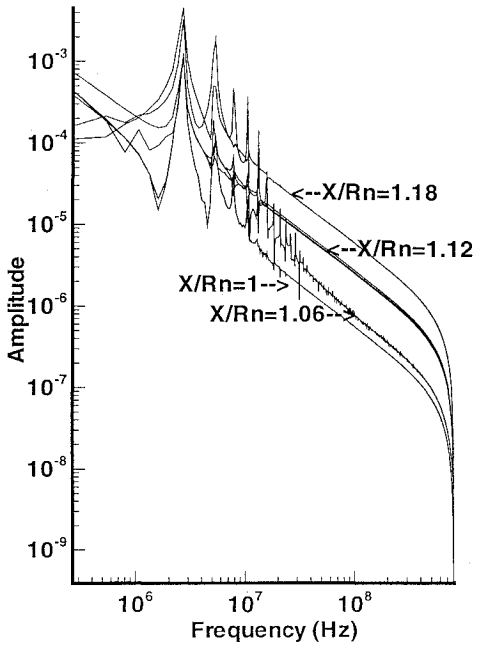

Fig. 5 Temporal frequency spectrum of water mass fraction for Mach 6.46 for 197 × 152 grid size.

are also shown. Thus, refining the grid from 131 × 101 to 197 × 152 has not significantly changed the frequency and, therefore, the oscillations in the reaction front are physical. Experimental fundamental frequency for the Mach 6.46 case is not available.

Conclusions

A numerical study is carried out to investigate the shock-induced combustion in premixed hydrogen-air mixture. The calculations have been carried out for Mach 5.11 and 6.46. The Mach 5.11 case was found to be unsteady with periodic oscillations. The frequency of oscillations was calculated and was found to be in good agreement with the experimentally observed frequency. The Mach 6.46 case was found to be of a very high frequency and very low-amplitude phenomena. Thus it can be considered as macroscopically stable. This supports the existing view that it is possible to stabilize the shock-induced combustion phenomena with sufficient level of overdrive.

References

[1]Lehr, H. F., "Experiments on Shock-Induced Combustion," *Acta Astronautica*, Vol. 17, Sept. 1972, pp. 586–589.

[2]Anonymous., Rapport-Bericht CO 7/73, Institut Franco-Allenmand De Recherches De Saint-Louis, Kolloquium Uber Gasdetonationen, obgehalten im ISL am 22.10.1973, ISL-Beitrage.

[3]Ahuja, J. K., and Tiwari, S. N., "Investigation of Hypersonic Shock-Induced Combustion in a Hydrogen-Air System," AIAA Paper 92-0339, Jan. 1992.

[4]Ahuja, J. K., and Tiwari, S. N., "Numerical Simulation of Shock-Induced Combustion in a Superdetonative Hydrogen-Air System," AIAA Paper 93-0242, Jan. 1993.

[5]Singh, D. J., Ahuja, J. K., and Carpenter, M. H., "Numerical Simulations of Shock-Induced Combustion/Detonation," *Computing Systems in Engineering*, Vol. 3, 1992, pp. 201–215.

[6]Wilson, G. J., and MacCormack, R. W., "Modelling Supersonic Combustion Using a Fully-Implicit Numerical Method," *AIAA Journal*, Vol. 30, No. 4, 1992, pp. 1008–1015.

[7]Sussman, M. A., "Source Term Evaluation for Combustion Modelling," AIAA Paper 93-0239, Jan. 1993.

[8]Wilson, G. J., and Sussman, M. A., "Computation of Unsteady Shock-Induced Combustion Using Logarithmic Species Conservation Equations," *AIAA Journal*, Vol. 31, 1993, pp. 294–301.

[9]Matsuo, A., and Fujiwara, T., "Numerical Simulations of Shock-Induced Combustion around an Axisymmetric Blunt Body," AIAA Paper 91-1414, June 1991.

[10]Matsuo, A., and Fujiwara, T., "Numerical Investigation of Oscillatory Instability in Shock-Induced Combustion around a Blunt Body," *AIAA Journal*, Vol. 31, 1993, pp. 1835–1841.

[11]Matsuo, A., Fujiwara, T., and Fujii, K., "Flow Features of Shock-Induced Combustion around Projectiles Travelling at Hypervelocities," AIAA Paper 93-0451, Jan. 1993.

[12]Ahuja, J. K., and Tiwari, S. N., "A Parametric Study of Shock-Induced Combustion in a Hydrogen-Air System," AIAA Paper 94-0674, Jan. 1994.

[13]McVey, J. B., and Toong, T. Y., "Mechanism of Instabilities of Exothermic Hypersonic Blunt-Body Flows," *Combustion Science and Technology*, Vol. 3, 1971, pp. 63–76.

[14]Jachimowski, C. J., "An Analytical Study of the Hydrogen-Air Reaction Mechanism with Application to Scramjet Combustion," NASA TP-2791, 1988.

[15]Drummond, J. P., Rogers, R. C., and Hussaini, M. Y., "A Detailed Numerical Model of a Supersonic Reacting Mixing Layer," AIAA Paper 86-1427, June 1986.

[16]MacCormack, R. W., "The Effect of Viscosity in Hypervelocity Impact Cratering," AIAA Paper 69-354, April–May 1969.

Observations on Using Experimental Data as Boundary Conditions for Computations

Paul D. Orkwis,* Chung-Jen Tam,† and Peter J. Disimile‡
University of Cincinnati, Cincinnati, Ohio 45221

Introduction

MANY computational efforts have been undertaken to simulate phenomena that have been studied experimentally. Numerous examples of this are found in the recent work on open cavity flows by Hankey and Shang,[1] Rizzetta,[2] Baysal et al.,[3] and others. These computations attempted to match the conditions of an experiment by employing the same nondimensional flowfield parameters, such as Mach and Reynolds numbers, and identical geometries. However, without intimate knowledge of the experimental procedures and apparatus it is impossible to match all of the boundary conditions for these flowfields. This knowledge includes the data collection procedures, the construction of the model, the proximity of the wind-tunnel walls, and the conditions outside of the test section. Researchers typically either ignore these details or assume an idealized configuration. This Note describes the procedures employed by the authors to determine computational boundary conditions from an experimental supersonic open cavity flowfield study and the observations made during this process.

Observations

An experimental and computational research program[4] has been undertaken to study the flow physics of supersonic open cavity flowfields such as those encountered by stealthy fighter, attack, and bomber aircraft. This effort requires a synergistic approach to acquire valid field and surface data because neither experimental nor computational methodologies are capable of efficiently producing both. Acquired experimental data include time-averaged surface pressures, time histories of surface pressures, upstream boundary-layer streamwise velocities, and qualitative surface streaking using shear stress sensitive liquid crystals. Computational data include time histories of all field properties. These computational data can then be time averaged and compared with the surface data obtained

Presented as Paper 94-0589 at the AIAA 32nd Aerospace Sciences Meeting, Reno, NV, Jan. 10–13, 1994; received July 13, 1994; revision received Sept. 12, 1994; accepted for publication Sept. 30, 1994.

*Assistant Professor, Department of Aerospace Engineering and Engineering Mechanics. Member AIAA.

†Research Assistant. Member AIAA.

‡Associate Professor, Department of Aerospace Engineering and Engineering Mechanics. Member AIAA.